CHALMERS
UNIVERSITY OF TECHNOLOGY

Surface active alkyl-imidazolium ionic liquids studied as templates to form vertically oriented pores in silica thin films

Journal of Molecular Liquids 353 (2022) 118686

Contents lists available at ScienceDirect

Journal of Molecular Liquids

journal homepage: www.elsevier.com/locate/molliq

Surface active alkyl-imidazolium ionic liquids studied as templates to form vertically oriented pores in silica thin films

Szilvia Vavra, Anna Martinelli *

Department of Chemistry and Chemical Engineering, Chalmers University of Technology, 412 96 Gothenburg, Sweden

ARTICLE INFO

Article history:
Received 21 October 2021
Revised 20 January 2022
Accepted 2 February 2022
Available online 19 February 2022

Keywords:
Surface Active Ionic Liquids (SAILs)
Electrochemically Assisted Self-Assembly (EASA)
Thin Films
Mesoporous Silica

ABSTRACT

In this study, thin films of mesoporous silica with vertically oriented and hexagonally ordered pores have been synthetized and investigated. A variety of alkyl-imidazolium ionic liquids have been used as the template, with the aim to understand how changing the chain length on the imidazolium cation from hexadecyl (C_{16}) to dodecyl (C_{12}) or the protic character of the imidazolium head affects the film formation and the order of the pores. In addition, different types of metal substrates have been used for the film deposition, i.e. indium titanium oxide (ITO) and gold. Complementary experimental methods, including GISAXS, Infrared spectroscopy, and cyclic voltammetry have been employed for a thorough investigation of the morphology and permeability of the deposited thin films.

1. Introduction

In the last two decades, the rapidly increasing research interest in ionic liquids (ILs) has not only lead to key findings on their structure and properties, widening the range of possible applications, but has also resulted in the exploration of new classes of ionic liquids and ionic liquid based multi-component materials. As this paper treats an emerging class of ionic liquids as silica templates, namely surface active ionic liquids (both protic and aprotic), these will be described in further details.

Surface active ionic liquids (SAILs), i.e. ionic liquids showing enhanced amphiphilic nature, are drawing interest as alternatives to conventional surfactants and mesogens, just as well as alternatives to short-chain ionic liquids [1–4]. Compared to conventional surfactants, imidazolium-based SAILs (Im-SAILs) can provide higher surface activity and more diversified aggregation behaviour [1]. Im-SAILs are also studied for applications already at focus for the wider class of imidazolium based ionic liquids, for example as electrolytes and catalysts [2,3,5]. The use as electrolytes is highly motivated by their non hygroscopic nature, as opposed to the case of many short-chain ionic liquids that readily absorb water from air leading to poorer electrochemical properties. Across the series of alkyl-methylimidazolium ionic liquids, [C_6mim][Cl] is known to be the 'transitional ionic liquid', showing surface activity but no self-assembly in water, while [$C_n$mim][Cl] ionic liquids with n>8 form micelles in water. Going further with the chain length, Im-SAILs can form liquid crystalline phases, as observed in e.g. [$C_n$mim][Br] when n>12 [4,6–9]. The ability of Im-SAILs to assemble can be extremely useful for applications; as a prominent example Su et al. have shown that the amphiphilic assembly of Im-SAILs leads to characteristic maxima in the differential capacitance [3].

Protic ionic liquids (PILs) are another subset of ionic liquids, that possess an acidic proton typically on the cation. They are prepared by a neutralization reaction between a Brønsted acid and a Brønsted base with sufficiently high ΔpK_a [10]. Based on the ease of this synthesis, PILs are often highlighted for being more affordable than their aprotic counterparts and hence advantageous for use in applications, e.g. as lubricants or electrolytes in supercapacitors [10–12]. However, the unique chemical structure of PILs, with the exchangeable protons, offers more functionalities; as an example, Xiao et al. have shown that the cycloaddition of CO_2 to epoxides can be catalysed by PILs with the reaction yield depending on the Hammett acidity [13]. Another crucial structural feature of PILs is the ability of the cation to form extended hydrogen-bonded networks with anions or other neutral compounds that can provide proton acceptor sites. These hydrogen-bonded networks may support a decoupled proton motion, such that the ionic conduction can occur not only by the vehicular mechanism (the charge being carried by the molecular species) but also by the Grotthuss or hopping mechanisms (the proton moving faster than the molecular species) [14]. Therefore, PILs are also extensively studied as proton conducting compounds for use in hydrogen fuel cells and other electrochemical devices [10].

For some applications (e.g., heterogeneous catalysis, solid-phase micro-extraction, and ion-conductive membranes), confinement of the ionic liquid into a solid (porous) matrix is a common

https://doi.org/10.1016/j.molliq.2022.118686
0167-7322/

approach to overcome the limitations that originate from the intrinsic liquid nature of ionic liquids [5,15–18]. In addition, it has been proven that ionic liquids can show improved performance upon confinement, due to the different chemical and steric environment provided by the matrix (e.g., higher catalytic activity and faster charge transport) [16,19]. For instance, Garaga et al. have achieved enhanced proton mobility by confining the [HC_8-Im][TFSI]/imidazole liquid mixture in the pores of hydrophobized mesoporous silica, a result that was rationalized by the occurrence of chain-chain assembly involving the octyl tails of the Im-SAIL and the octyl groups of the silica pore walls [19].

In parallel to the increased research activity aimed to understand the structure–properties correlation in ionic liquids under confinement, various confining methods have also been developed. IL/silica hybrid materials, in which the ionic liquid is confined in the meso- or macro-pores of the silica matrix, can be prepared by *in situ* synthesis during which the confining matrix evolves in the presence of the ionic liquid [5,18]. An alternative way is by impregnating the pre-synthetized porous solid matrix with the ionic liquid of choice [5,18,20,21]. The former has indeed the advantage of being a one-step method, although templating silica with ionic liquids is not straightforward. Imidazolium based ionic liquids have drawn increasing attention as suitable soft-templates for the realization of mesoporous silica structures, enabling to tune the pore morphology by the reaction condition and the molecular structure of the ionic liquid itself [22–28]. For example, [$C_n$mim][BF_4] ionic liquids with an intermediate chain length (n = 4, 6, 8) can be used to form non-ordered, worm-like pores in monolithic amorphous silica under acidic conditions [24,25], whilst for more ordered pore structures [$C_n$mim][Cl] ionic liquids with longer chains are needed. Under acidic conditions, the lamellar structure in monolithic silica can be achieved using [C_n-mim][Cl] with long chains (n = 14–18) [23,27]. Under basic conditions, on the other hand, [$C_n$mim][Cl] with n = 8–12 form worm-like pores, while the longer chain ionic liquids [C_{14}mim][Cl] and [C_{16}mim][Cl] do form ordered hexagonal structures [26,29]. The ionic liquid [C_{16}mim][Cl] is suitable to form hexagonally ordered channel-like pores not only in monolithic silica, but also in thin films of silica during the electrochemically assisted self-assembly (EASA) that results in vertically aligned pores [30]. Such vertical alignment is especially advantageous for applications in which transport phenomena have an important role. It is noteworthy that even though the EASA method is used for the synthesis of thin films (as is the case of this study), with sufficiently long deposition times the formation of templated silica particles aggregating on the film's surface can also be observed [28,31].

This study aims to explore the possibilites and limitations of protic and aprotic SAILs when used to template thin films of silica *via* the EASA method. To investigate the effect of the chain length on the templating behaviour, the ionic liquid series [$C_n$mim][Cl] with n varied from 12 to 16 was considered, while the incorporation of the protic head was studied using [HC_{16}Im][Cl]/[C_{16}mim][Cl] mixtures of different composition. The synthetized materials were chemically and morphologically characterized by GISAXS, Infrared spectroscopy and cyclic voltammetry.

2. Experimental

For the synthesis of the ionic liquid-templated mesoporous silica thin films, the following reagents were used: tetraethyl orthosilicate (TEOS, 98%, Sigma–Aldrich) as the precursor; ethanol (EtOH, 99.5%, Solveco) as the co-solvent; sodium nitrate ($NaNO_3$, 99%, Sigma–Aldrich) as the salt electrolyte; and 0.1 M HCl in aqueous solution ($HCl_{(aq)}$, VWR) for pH adjustment. As silica templates, various ionic liquids were used, including aprotic and protic ones; the aprotic ionic liquids were 1-hexadecyl-3-methylimidazolium chloride (C_{16}mimCl, >98%, Iolitec - Ionic Liquid Technologies GmbH), 1-tetradecyl-3-methylimidazolium chloride (C_{14}mimCl, >98%, Iolitec - Ionic Liquid Technologies GmbH) and 1-dodecyl-3-methylimidazolium chloride (C_{12}mimCl, >98%, Iolitec - Ionic Liquid Technologies GmbH), while the protic ionic liquid was 1-hexadecylimidazolium chloride (HC_{16}imCl, >98%, Iolitec - Ionic Liquid Technologies GmbH). For the extraction of the templating ionic liquid from the pores, an ethanol solution of 0.1 M HCl was used, prepared by dilution of nominally 2.5 M HCl in ethanol ($HCl_{(EtOH)}$, Alfa Aeasar). The redox-probes used during cyclic voltammetry were hexaammineruthenium(III) chloride ($[Ru(NH_3)_6]Cl_3$, 98%, Sigma Aldrich), potassium hexacyanoferrate(III) ($K_3[Fe(CN)_6]$, >99.0%, Sigma–Aldrich), and α-methylferrocenemethanol (FcMeOH, 97%, Sigma–Aldrich). For cleaning the gold substrate, a 32% ammonia solution (NH_4OH, Sigma Aldrich) and a 30% hydrogen peroxide solution (H_2O_2, Sigma–Aldrich) were used; while for the surface treatment (3-mercaptopropyl) trimethoxysilane (MPTMS, 95%, VWR) was used. All aqueous solutions were prepared with Milli-Q water.

2.1. Sample preparation

The synthesis of the ionic liquid (IL)-templated mesoporous silica thin films was carried out *via* the electrochemically assisted self-assembly (EASA) method [32,33], depositing the films over an ITO-covered glass slide (surface resistivity of 8–12 Ω, Delta Technologies) or a gold-covered glass chip (Sofchip, Cat. No. 1000004–3). The gold electrode was carefully cleaned and surface treated before use. During cleaning, the gold chips were submerged in a 1:1:5 (V/V) mixture of 32% NH_4OH:30% H_2O_2:Milli-Q water at 80–90 °C for 10 min, then rinsed with Milli-Q water and blown with nitrogen. The surface treatment with MPTMS was carried out as described by Sibottier et al. [33]. The reaction solution for silica deposition contained 100 mM TEOS, 0.1 M $NaNO_3$, and 0.32 mM or 0.50 mM of the templating IL(s) (as summarized in Table 1) in a 40 ml ethanol:water (1:1) mixture, and was adjusted to pH 3 with 0.1 M $HCl_{(aq)}$. To ensure the prehydrolysis of TEOS, this solution was stirred for 2.5 h at room temperature.

The silica films were deposited from the hydrolysed reaction solution potentiostatically on the cathodic working electrode, in a three-electrodes cell using various potentials and deposition times, as listed in Table 1; for this electrochemical deposition a Gamry Interface 1000E potentiostat was used. The working electrode was an ITO-covered glass slide or a gold-covered glass chip, while a silver wire was used as the pseudo-reference electrode and stainless steel as the counter electrode. It is important to note that deposition over gold substrates could not be achieved at −1.55 V, and the applied voltage had to be increased to −1.60 V instead. The currents delivered during deposition were always recorded; as an example, the typical amperometric curves obtained during EASA using an ITO substrate and different alkylmethylimidazolium ionic liquids are presented in Figure S1.

After deposition, the films were rinsed with water, blown with nitrogen gas, and aged overnight at 130 °C in a vacuum oven. For some of the samples, the extraction of the ionic liquid was carried out by immersing the deposited film into a 0.1 M $HCl_{(EtOH)}$ solution for 20 min, followed by rinsing with pure ethanol and drying for 2 h in a vacuum oven at 90 °C. For consistency and clarity in the discussion that follows, the extracted films are labelled 'E' while 'NE' is the label for the not-extracted films.

Table 1
Sample names and other important parameters related to their synthesis.

Sample name	Templating IL	IL/TEOS ratio mol:mol	Substrate	Deposition voltage	Deposition time
MC12 0.5 I	C_{12}mimCl	0.50	ITO	−1.55 V	25 s
MC14 0.5 I	C_{14}mimCl	0.50	ITO	−1.55 V	25 s
MC16 0.5 I	C_{16}mimCl	0.50	ITO	−1.55 V	25 s
MC16 0.5 G	C_{16}mimCl	0.50	gold	−1.60 V	20 s
MC16 0.32 G	C_{16}mimCl	0.32	gold	−1.60 V	20 s
10H/MC16 0.32 G	10 mol% HC_{16}imCl 90 mol% C_{16}mimCl	0.32	gold	−1.60 V	20 s
30H/MC16 0.32 G	30 mol% HC_{16}imCl 70 mol% C_{16}mimCl	0.32	gold	−1.60 V	20 s

2.2. Infrared spectroscopy

The Infrared spectra of the thin mesoporous films were collected with a PerkinElmer Fourier transform Infrared (FT-IR) spectrophotometer using a Spectra-Tech FT-80 Fixed 80 °C Grazing Angle Accessory with all-reflective optical design, including gold mirrors that allow obtaining transmission spectra of the thin films. The measured spectral range was from 4000 cm^{-1} to 400 cm^{-1}, and the spectral resolution was 4 cm^{-1}. For each experiment, 64 scans were collected and averaged while the spectrum of an ITO substrate without any deposited film on it was used as a reference for the background subtraction. The Infrared spectra of the pristine ionic liquids were obtained in the ATR (attenuated total reflectance) mode using a GladiATR accessory with a single-reflection diamond crystal (Pike Technologies). The measured spectral range was from 4000 cm^{-1} to 400 cm^{-1}, the resolution was 4 cm^{-1}, and 32 scans were collected and averaged for each acquisition. For presentation purposes, all the recorded Infrared spectra were baseline corrected and then normalized to the highest absorption peak observed.

2.3. X-ray scattering

The pore morphology of the thin films was studied with grazing incidence small angle X-ray scattering (GISAXS) measurements, performed on a Mat:Nordic instrument from SAXSLAB/Xenocs. The incident X-ray beam was generated by a Cu-radiation source and focused with a Micro-Max 003 X-ray generator from Rigaku. The scattered rays were collected with a Pilatus 300 K detector from Dectris. The samples were placed on a GISAXS holder and aligned before each measurement, first automatically and then manually for a higher precision. The sample-to-detector distance was set to 314 mm, the incidence angle to 0.2°, and the exposure time to 6 h. The collected 2D scattering patterns were further processed with the SAXSGUI (Rigaku) software, and the horizontal integration of intensities between q_z=0.01 $Å^{-1}$ and q_z=0.05 $Å^{-1}$ are presented as a function of q_y (the horizontal integration of the 2D X-ray scattering pattern is shown for one example sample in Figure S2). To determine exact peak positions, the data were further processed by multi-peak fitting in the Igor software using Voigt components. The cell parameters were determined from the size of the scattering objects based on their observed structural correlation length, d, where $d = 2\pi/q_{max}$ and q_{max} is the position of the scattering peak [34].

2.4. Cyclic voltammetry

The permeability of the deposited films was investigated by cyclic voltammetric measurements using various coordination compounds as redox-probes, selected to have different and characteristic electrochemical properties. More precisely, the positive redox-probe hexaammineruthenium(III) chloride ($[Ru(NH_3)_6]Cl_3$), the negative redox-probe potassium hexacyanoferrate(III) ($K_3[Fe(CN)_6]$), and the neutral redox-probe α-methylferrocenemethanol (FcMeOH) were used. All measurements with the different redox-probes were carried out in a three-electrodes system containing a stainless steel counter electrode, a Ag/AgCl reference electrode (Pine Research Instrumentation, Inc.), and a bare ITO plate or an ITO plate with the deposited silica film on it as the working electrode. The aqueous electrolyte contained 0.5 mM redox-probe and 0.1 M $NaNO_3$, while the contact area of the working electrode with the electrolyte solution was 0.2 cm^2 (defined by the size of the o-ring used to seal the electrochemical cell). The voltammogram curves were recorded with a Gamry Interface 1000E potentiostat at a scan rate of 20 mV/s.

3. Results and discussion

3.1. Decreasing the alkyl chain length

Based on chemical, morphological and permeability characterization, we find that it is possible to template thin films of mesoporous silica, synthetized *via* the electrochemically assisted self-assembly (EASA) method with alkyl-methylimidazolium based ionic liquids bearing a shorter alkyl chain than the ionic liquid previously reported, i.e. hexadecyl-methylimidazolium chloride (C_{16}mimCl) [28]. More precisely, we find that decreasing the length of the alkyl chain in the templating alkyl-methylimidazolium ionic liquid from hexadecyl (C_{16}) to tetradecyl (C_{14}) still results in the formation of vertically aligned channel-like mesopores extending through the entire film thickness, whereas an abrupt loss of the templating function was observed when the alkyl chain of the ionic liquid was decreased to the dodecyl group (C_{12}).

Infrared spectroscopy. The Infrared spectra of the silica films synthetized using alkyl-methylimidazolium ionic liquids with different alkyl chain lengths are shown in Fig. 1, along with the spectra of the corresponding, bulk ionic liquids. The characteristic Infrared absorption peaks of the C_{16}mimCl and C_{14}mimCl ionic liquids originate from the symmetric and antisymmetric C–H stretching modes in the alkyl chain (2960–2850 cm^{-1}) and from the bending modes in the imidazolium ring (1570 cm^{-1}, 1170 cm^{-1}). The appearance of these vibrational modes also in the spectra of the corresponding silica thin films (i.e., the NE samples) demonstrates the presence of these ionic liquids in the deposited films [28,35]. Furthermore, the drastic decrease of these absorption peaks upon extraction (E samples) confirms the effective removal of the templating ionic liquid and indicates that instead of being immobilized in the silica network, the ionic liquids are in the pores and thus accessible to the extraction solution. Contrarily to the cases of C_{16}mimCl and C_{14}mimCl, the shorter chained ionic liquid C_{12}mimCl is not incorporated in detectable amounts into the silica thin film during EASA, as can be concluded from the absence of the characteristic peaks of C_{12}mimCl in the Infrared spectrum of the corresponding film (top-most traces in Fig. 1).

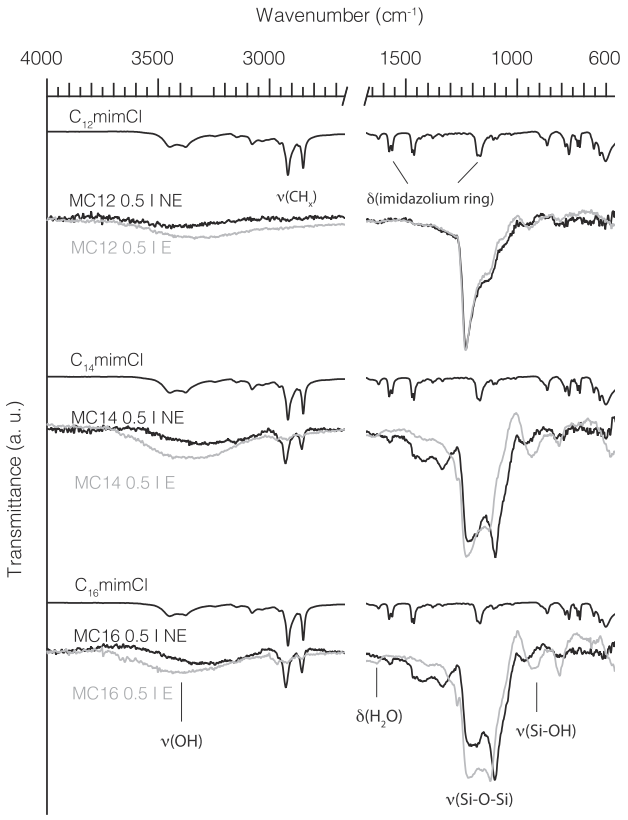

Fig. 1. Infrared spectra of the silica thin films synthetized using alkyl-methylimidazolium ionic liquids with varying chain lengths. The annotation 'NE' stands for samples before extraction (i.e., not-extracted) while 'E' stands for extracted samples. The Infrared spectra have been vertically offset for a clearer visualization.

A number of overlapping absorption peaks are observed in the spectral region 1250–1000 cm^{-1} of the infrared spectra recorded for the silica thin films; these are characteristic of sol–gel derived silica networks and reveal that during EASA the silica deposition proceeded in the presence of all the three investigated alkyl-methylimidazolium ionic liquids. Even though all the deposited films show to consist in an amorphous, condensed siliceous network, the characteristic vibrational modes of silica show distinctive differences; in particular, the Infrared spectrum of the film deposited using C_{12}mimCl is slightly different than the spectra recorded for the films prepared using either C_{14}mimCl or C_{16}-mimCl. The latter two spectra are also similar to the spectrum of C_{16}mimCl-templated films previously reported by us [28].

A more elaborated description of the structural features of the synthetized silica thin films can be retrieved from the recorded Infrared spectra, although the peak assignment of the 1250–1000 cm^{-1} region is not straightforward [36–39]. One important detail is the absence of the absorption peak at 1100 cm^{-1} in the spectrum of the MC12 0.5 I NE sample, a peak that is characteristic of the stretching modes of siloxane bonds in linear silica units [38]. Björk et al. have recently reported an *in situ* Infrared spectroscopic study during silica condensation, revealing that as the condensation proceeds the stretching vibration peak of linear silica units decreases simultaneously to the increase of the absorption peak at 1200 cm^{-1}, attributed to the stretching modes of sixfold silica rings [38]. It can thus be proposed that the higher ratio between the Infrared absorption at 1200 cm^{-1} and that at 1100 cm^{-1} indicates that the MC12 0.5 I NE sample consists of a more condensed and/or continuous silica network than the MC14 0.5 I NE or the MC16 0.5 I NE samples. This can also explain the slight relative decrease of the absorption peak at 1100 cm^{-1} upon extraction, since this is performed at acidic pH followed by mild heat treatment, which both can promote further condensation of unreacted silanol and ethoxy groups. Also notable is the blue shift of the mentioned vibrations after extraction, which indicates a moderate increase of the average Si-O-Si angles in the silica network [40]. In addition, it is important to remind that besides these two vibrational modes other vibrations should be considered, for instance those contributing at 1040, 1160, and 1250 cm^{-1} arising from other stretching modes of the siloxane bonds in the silica network [36–38,40].

Moreover, silanol groups are part of the siliceous network as revealed by the characteristic absorption peak at 950 cm^{-1} attributed to Si-OH stretching. These hydroxyl groups contribute also around 3500 cm^{-1} (SiO-H stretching), a region that overlaps with the O-H stretching modes of water. Further, the presence of absorbed water is also indicated by its characteristic mode at around 1630 cm^{-1} assigned to H-O-H bending [36].

GISAXS. The X-ray scattering patterns collected from the studied thin films reveal distinct differences in the pore morphology between the samples, in agreement with the results from Infrared spectroscopy. The thin films templated by C_{14}mimCl and C_{16}mimCl show similar patterns and a pore structure consisting of hexagonally ordered, vertically aligned channel-like mesopores, while the use of C_{12}mimCl during EASA does not result in such a porous, ordered structure, see Fig. 2 (and Table S1). Moreover, an important structural feature is that the cell parameter of the film templated by C_{14}mimCl is smaller than that of the film templated by C_{16}mimCl, which reflects mesochannels with a smaller pore diameter [41].

Among the peaks appearing along the horizontal axis of the 2D scattering pattern of the films templated by C_{14}mimCl and C_{16}-mimCl, presented in Fig. 2, the following ones can be assigned to

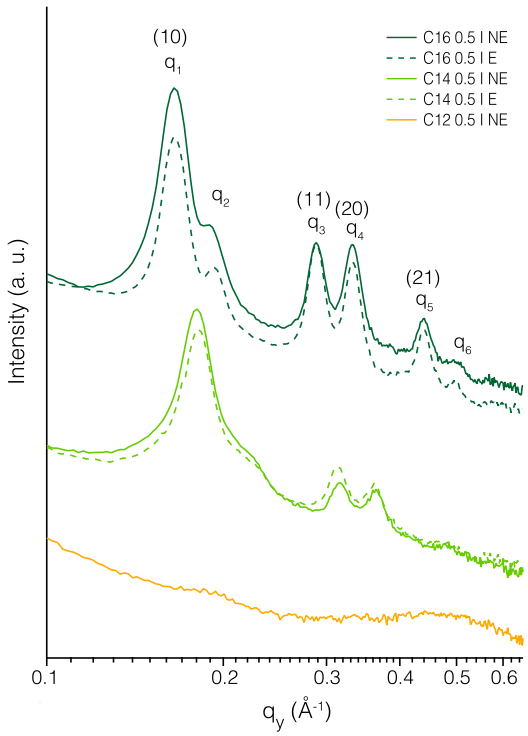

Fig. 2. X-ray scattering intensities integrated along the horizontal axis attained from the 2D scattering patterns recorded for different mesoporous silica thin films. The annotation 'NE' stands for samples before extraction (i.e. not-extracted) and 'E' for samples after extraction.

the Miller indices of the long-range hexagonally ordered pore structure formed: q_1(10), q_3(11), q_4(20), and q_5(21), which have a peak position ratio of $1:\sqrt{3}:\sqrt{4}:\sqrt{7}$ characteristic of the hexagonal p6m symmetry of the channel-to-channel spacing [42,43]. The cell parameter of the C_{16}mimCl-templated silica films is 4.4 nm, while the change of the templating ionic liquid to C_{14}-mimCl resulted in a cell parameter decreased to 4.0 nm. Referring to the work of Zienkiewicz-Strzaka et al., and considering that the ratios of the scattering intensities of the (11) and (20) reflections (i.e., the ratio I(11)/I(20)) are very close in the C_{16}mimCl- and the C_{14}mimCl-templated films (1.01 and 1.11 respectively), it can be concluded that the morphology of the pores and the silica walls is similar; the only difference being the smaller unit cell parameter and hence an overall smaller pore structure [41].

In addition, the scattering intensity peaks superimposed on the peaks of the planar hexagonal lattice reflections, namely the peaks labeled q_2 and q_6 in Fig. 2, originate from the porous silica particles located on top of the films' surface (see also SEM images in Figure S3) [28,43]. The formation of such particles is common during the EASA synthesis of silica thin films, as a consequence of the pH gradient formed at the surface of the working electrode resulting in the condensation of silica also in the bulk of the reaction solution close to the surface [43]. The ratio between the peak areas belonging to q_1 and q_2 was calculated to be lower for the C_{14}mimCl-templated silica film than for the C_{16}mimCl-templated one (A_1/A_2 in Table S1), which can possibly be rationalized by a relatively lower amount of particles on top of the C_{14}mimCl-templated silica film. Sample-to-sample differences may be expected although the SEM images of the samples presented in Figure S3 do not reveal major variations. Also, a systematic increase of the A_1/A_2 value after the extraction procedure is noticed, which indicates a partial removal of the particles from the film's surface.

Differently to the case of using C_{14}mimCl or C_{16}mimCl, the use of the shorter chain ionic liquid C_{12}mimCl resulted in a silica film whose X-ray scattering pattern does not show any of the intensity peaks characteristic of the hexagonally ordered, vertically aligned mesochannels. In the full scattering range associated to the nanometer-scaled correlation lengths, the 2D scattering pattern of the C12 0.5 I NE sample contains only one weak-intensity ring with a peak maximum at 0.19 $Å^{-1}$ (d = 3.4 nm). The assignment of this peak is not straightforward as it can arise from both the silica network and the chain-chain separation of the self-assembled ionic liquid, which may be present in trace amounts (thereby not detectable by Infrared spectroscopy). Interestingly, the SEM images (see micrographs in Figure S3) seem to reveal a lower amount of particles on the surface of this film than in the case of C_{14}mimCl and C_{16}mimCl-templated films. Altogether, all these results are in line with those achieved by Infrared spectroscopy, suggesting that the silica film deposited *via* EASA using C_{12}mimCl consists of amorphous and condensed, but non-porous silica.

Cyclic voltammetry. As an additional characterization method to reveal the pore morphology in the silica thin films, cyclic voltammetry with various redox-probes has been applied, which provides information on the permeability of the films, Fig. 3. The C_{16}mimCl-templated silica thin film containing hexagonally ordered, vertically aligned channel-like pores filled with the ionic liquid is not permeable to the positively charged $[Ru(NH_3)_6]^{3+}$ and negatively charged $[Fe(CN)_6]^{3-}$ redox-active complexes. In other words, the lack of redox-peaks reveals that the diffusion pathway towards the ITO electrode is blocked by the deposited film. Thus, before extraction the C_{16}mimCl-templated film behaves as an insulator layer for both positive and negative redox-probes revealing that the deposited film covered the entire contact area. However, the neutral redox-probe α-methylferrocenemethanol, having a Fe(III)-ion complexed with cyclopentadienyl rings, is likely to solubilize in the apolar phase of the assembled ionic liquid located in the pores, hence able to reach the ITO electrode giving rise to a shifted, but strong oxidation peak [44]. After extraction, the positive redox-probe and the neutral-redox probe can pass through the silica film *via* the emptied mesochannels, resulting in reduction and oxidation peaks on the cyclic voltammetric curves that resemble the current response measured with a bare ITO substrate. This behaviour is similar to that previously reported for C_{16}-mimCl-templated [28] and CTAB-templated [32,44] silica films. On the other hand, the negative redox-probe $[Fe(CN)_6]^{3-}$ could not reach the ITO electrode even after extraction, which is explained by the negatively charged silica pore walls repelling this redox-probe, again indicating a good coverage of the film [44].

Although the C_{14}mimCl-templated and C_{16}mimCl-templated silica thin films show similar vibrational spectra and X-ray scattering patterns, there is a slight difference in their cyclic voltammetric response. Specifically, on the cyclic voltammetric curves obtained with the $[Ru(NH_3)_6]^{3+}$ solution the non-extracted C_{14}mimCl-templated silica film deposited on the ITO electrode shows small but measurable current peaks of reduction and oxidation, suggesting defects in the film. Considering that before the extraction of the film the oxidation peak of the neutral redox-probe FcMeOH is shifted, reflecting a hindered diffusion, and that after extraction the $[Fe(CN)_6]^{3-}$ does not show Faradaic currents, it can be proposed that instead of larger damages (for example macroscopic scratches) the size of the defects in the film is rather comparable to the size of the used redox-probes. Thus, based on the work of Sibottier et al. [33], the higher current of the voltammetric curve measured with the $[Ru(NH_3)_6]^{3+}$ solution for the non-extracted C_{14}mimCl-templated silica film can indicate that the film is thinner and more permeable possibly due to a slower growth in the presence of C_{14}mimCl.

Judging from the cyclic voltammetric results, the formation of a highly condensed, continuous silica film has been found when the silica is deposited *via* EASA in the presence of C_{12}mimCl. Independently of the type of redox-probe used, no Faradaic currents were measured neither before nor after the extraction procedure, showing that the silica film acts as an insulating layer on top of the ITO electrode.

The abrupt loss in templating function of alkylmethylimidazolium ionic liquids when the alkyl chain is decreased to the length of a docedyl group is congruent with previous studies carried out on EASA with alkyl-trimethylammonium bromide (alkyl-TAB) compounds by Goux et al. [45]. That is, while C_{14}TAB can still form hexagonally-ordered and vertically-aligned mesochannels in the deposited silica film, in the presence of C_{12}TAB the silica film is described to be mesostructurally not ordered. An interesting similarity between the $C_n$mimCl and C_nTAB families is that their critical micelle concentrations (cmc) are very close: 4 mM for both C_{14}mimCl and C_{14}TAB, while 15 mM for C_{12}-mimCl and 16 mM for C_{12}TAB [7,46,47]. Thus, it can be concluded that there is a correlation between solubility and pore-forming function of the templating amphiphile; nevertheless there are other vital factors that also determine the formation of a mesoporous silica structure, such as the interaction between the silica precursor and the templating agent [28].

3.2. Changing the substrate

Changing the deposition substrate from ITO to gold is just as viable in the case of C_{16}mimCl-templated silica films as for CTAB-templated ones [33]. In fact, the same pore morphology is obtained, consisting in hexagonally-ordered and verically-aligned mesopores throughout a continuous film of amorphous silica. By comparing the C_{16}mimCl-templated films deposited on either ITO

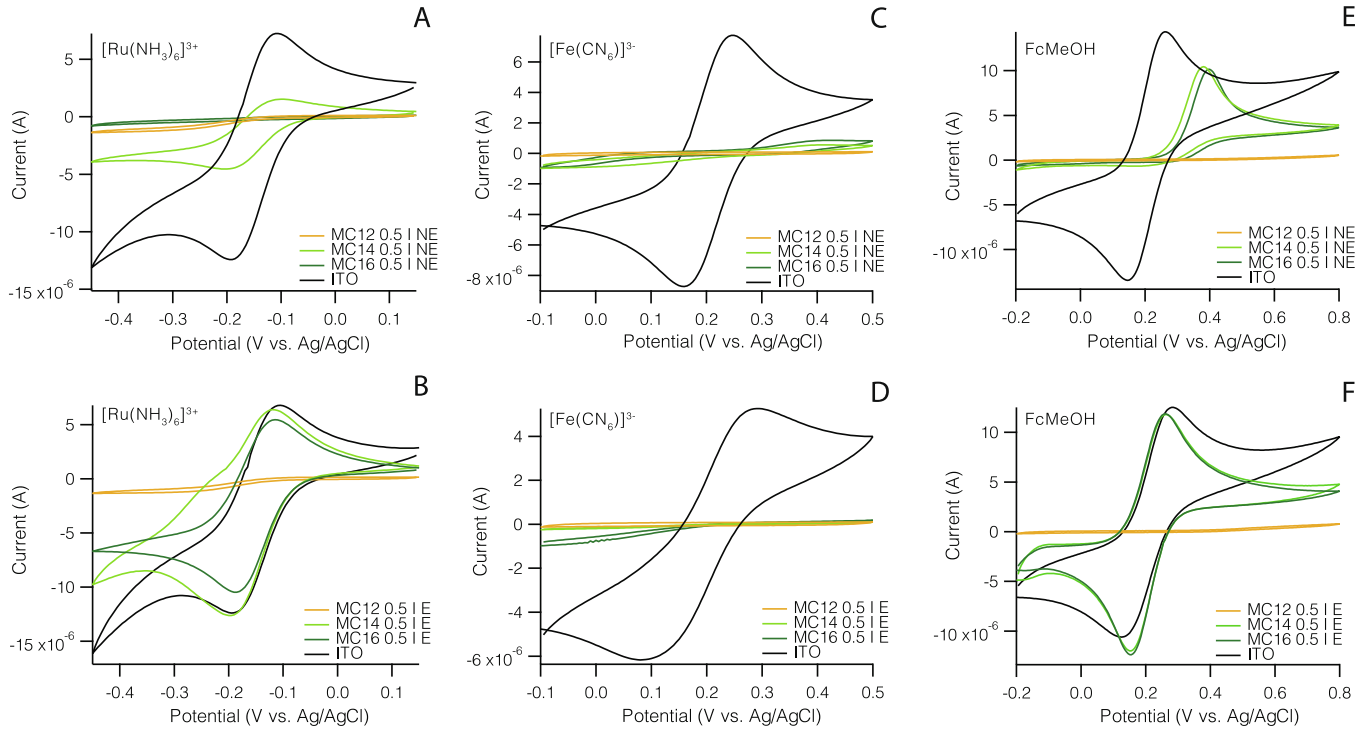

Fig. 3. Cyclic voltammetric curves recorded with a positive redox-probe $[Ru(NH_3)_6]Cl_3$ solution (A-B), a negative redox-probe $K_3[Fe(CN)_6]$ solution (C-D), and a neutral redox-probe FcMeOH solution (E-F) using a bare ITO electrode and ITO electrodes covered with the IL-templated silica thin films, before (A, C, E) and after (B, D, F) extraction of the ionic liquid.

or a gold substrate at different settings (samples MC16 0.5 I, MC16 0.5 G, and MC16 0.32 G) we observe that their Infrared spectra are so similar that they must arise from the same type of silica network (see Fig. 1 and Figure S4; the detailed analysis of the vibrational absorption peaks related to the ionic liquid and the silica network has already been discussed above). Furthermore, C_{16}mimCl is present as a templating agent and can be removed upon extraction. Their cyclic voltammetric curves are also similar, showing that the films are continuous and that after removal of the ionic liquid the emptied mesochannels are permeable to the positive and neutral redox-probes (see Fig. 3 and Figure S5). A minor, but measurable difference between these samples is that even though they all consist in hexagonally-ordered mesochannels, the cell parameter increases slightly by changing the substrate from ITO to gold and by decreasing the IL/TEOS ratio (see Figure S6 and Table S2). Interestingly, it can be observed that for the samples with a higher cell parameter the current recorded during deposition was higher, Fig. 4. Since during EASA the electric current drives water electrolysis resulting in a pH gradient close to the electrode's surface, it can be speculated that the higher current is related to a higher pH at the electrode hence influencing the base-catalyzed condensation of the silica network and the pore formation.

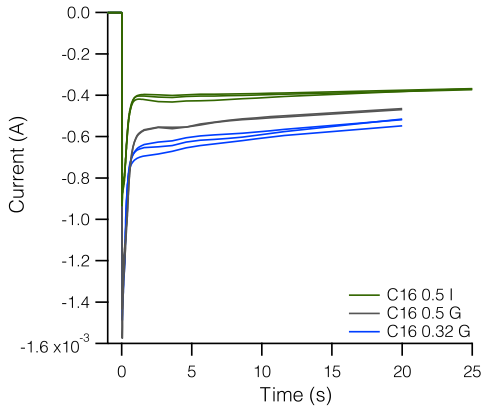

Fig. 4. Current delivered during the deposition of silica thin films *via* the EASA method. The applied voltage was −1.55 V in the case of deposition onto ITO (MC16 0.5 I) and −1.60 V in the case of deposition onto a gold substrate (MC16 0.5 G, MC16 0.32 G).

3.3. Mixing protic and aprotic Im-SAILs

Based on the chemical and morphological characterization, we find that the protic ionic liquid HC_{16}imCl does not function as a templating agent during EASA of silica thin films. To arrive at this conclusion, the EASA method was tested using HC_{16}imCl/C_{16}mimCl mixtures of different composition, see also Table 1. First of all, it is important to mention that the reaction solution containing solely HC_{16}imCl as the templating ionic liquid could not be prepared at all, as the necessary amount of HC_{16}imCl did not dissolve and the reaction solution remained opaque. The following depositions were therefore carried on using this protic ionic liquid mixed with the aprotic ionic liquid C_{16}mimCl (already known to have a templating function).

While synthetizing silica thin films in the presence of 0, 10, and 30% of HC_{16}imCl in the HC_{16}imCl/C_{16}mimCl mixture, a net change in the type of obtained silica network and pore morphology was observed upon increasing the HC_{16}imCl content. Samples prepared with 0% (C16 0.32 G NE) and 10% (10H/MC16 0.32 G NE) of HC_{16}imCl in the HC_{16}imCl/C_{16}mimCl mixture show similar Infrared spectra (see Figure S7) and X-ray scattering patterns (Fig. 5 and Table S3). In the spectral region 1250–1000 cm^{-1}, the Infrared spectra show the characteristic absorption peaks of amorphous silica networks, similarly to the case of the C_{16}mimCl-templated films

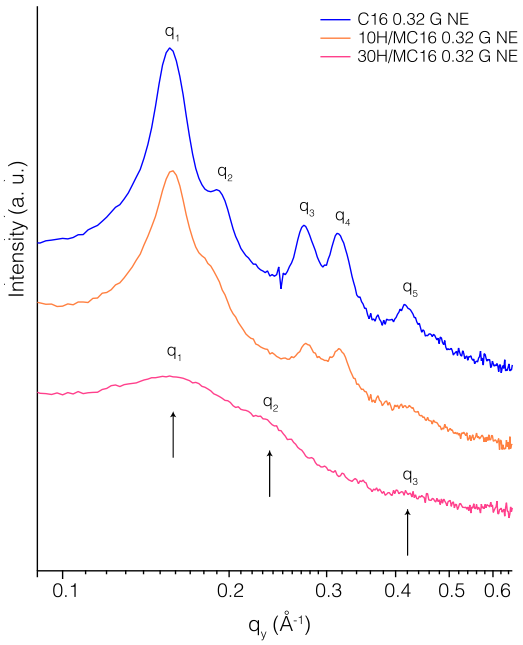

Fig. 5. X-ray scattering intensities integrated along the horizontal axis of the 2D scattering patterns of mesoporous silica thin films deposited with the EASA method in the presence of varying HC_{16}imCl/C_{16}mimCl mixtures.

discussed above. Also, upon extraction the spectral changes indicate a further condensation of the silica network. The strong absorption peaks arising from the hexadecyl-chain appear in the spectra of both sample C16 0.32 G NE and sample 10H/MC16 0.32 G NE; however for the latter the presence of the protic ionic liquid HC_{16}imCl could not be explicitly confirmed. Interestingly, the X-ray scattering of these two samples show that they are not only identical, with respect to the hexagonally-ordered and vertically-aligned channel-like pores, but also have equal cell parameters within the measurement's error. Despite this morphological equivalence, the cyclic voltammetric response of these two samples is different, Fig. 6. More precisely, in the case of the sample 10H/MC16 0.32 G smaller currents were recorded from the redox reactions of the positive and neutral redox-probes, despite results from Infrared spectroscopy confirm a successful extraction. Since the presence of particle aggregates on the top of the film is not excessive (based on the A_1/A_2 value reported in Table S3) and the CV curve recorded with the negative redox-probe indicates an intact film, the recorded small currents of positive and neutral redox-probes may originate from a slower mass transport through the pores, which in turn can be related to a lower porosity [45] or obstructed pores.

By contrast, when the templating ionic liquid mixture contains 30% of HC_{16}imCl, namely in the case of sample 30H/MC16 0.32 G NE, the Infrared absorption spectrum of the silica network shows, in the region 1250–1000 cm^{-1}, features resembling those of a non-porous, more condensed silica film (compare Figure S7 with Fig. 1). Nevertheless, the presence of the ionic liquid within the structure is evidenced by the alkyl chain absorption peaks, that disappear upon extraction revealing that the incorporated ionic liquid is not immobilized within the silica network. Similarly to sample 10H/MC16 0.32 G NE, also for sample 30H/MC16 0.32 G NE the co-presence of the protic HC_{16}imCl and the aprotic C_{16}mimCl could not be verified. In the same time, the X-ray scattering pattern does not show the formation of hexagonally-ordered, vertically-aligned channel-like pores but rather non-ordered scattering intensities with nanometer-scale correlation lengths of 4.0 nm, 2.7 nm, and 1.4 nm. These can originate from the electron-density contrast of apolar/polar nanostructuration of self-assembled ionic liquids but also possible repetitiveness of these assemblies. In addition, cyclic voltammetric measurements showed that even though the ionic liquid forms pores within the silica film, these do not extend

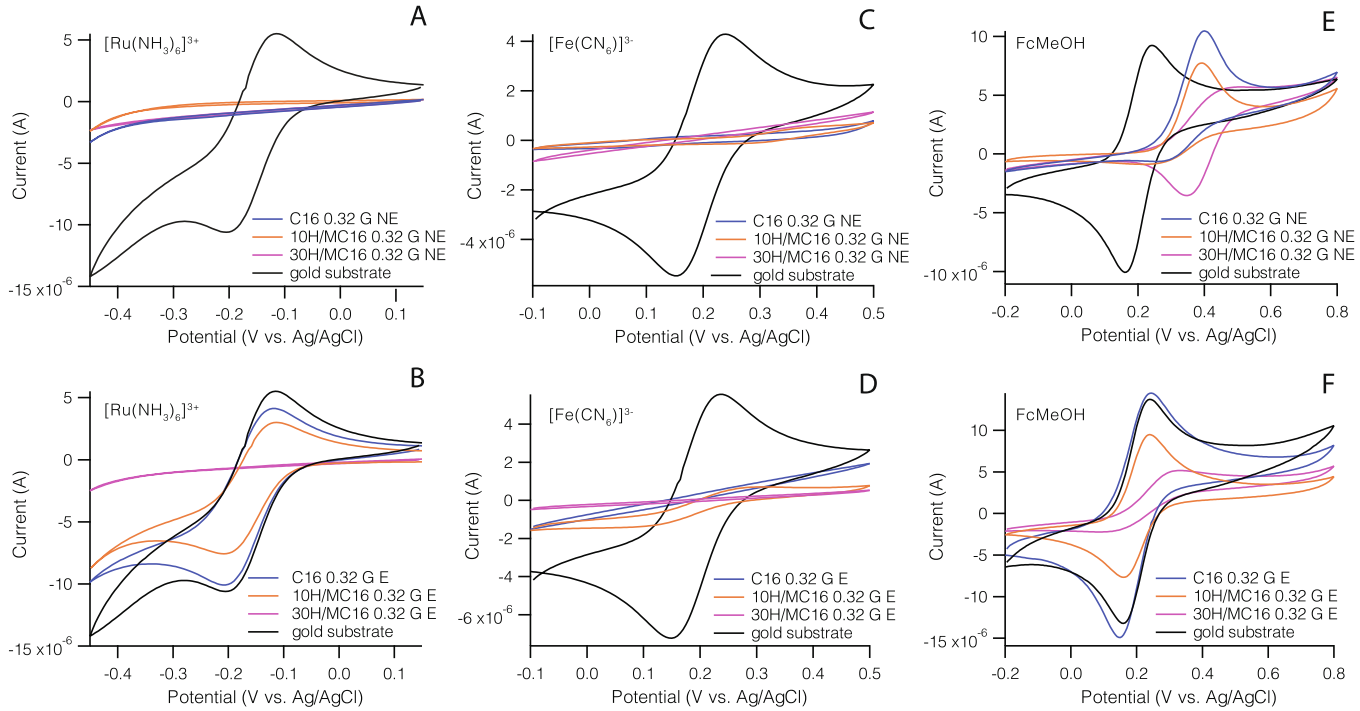

Fig. 6. Cyclic voltammetric curves recorded in a positive redox-probe $[Ru(NH_3)_6]Cl_3$ solution (A-B), negative redox-probe $K_3[Fe(CN)_6]$ solution (C-D), and neutral redox-probe FcMeOH solution (E-F) using a bare gold electrode and gold electrodes covered with the IL-templated silica thin films synthetized in the presence of HC_{16}imCl/C_{16}mimCl mixture with various composition ratios, before (A, C, E) and after (B, D, F) extraction of the ionic liquid.

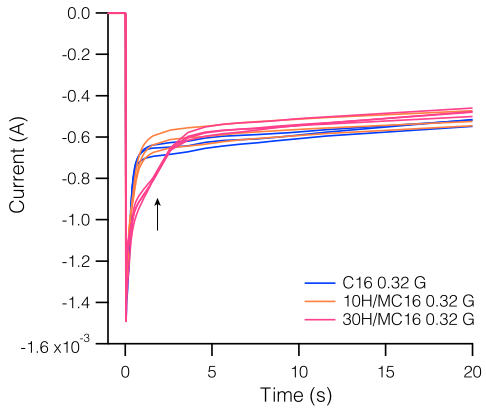

Fig. 7. Current delivered during the deposition of silica thin films *via* the EASA method in the presence of HC_{16}imCl/C_{16}mimCl mixtures, showing the cases of 0%, 10% and 30% of HC_{16}imCl. The arrow indicates an additional current observed solely when using the protic ionic liquid.

through the entire thickness of the film as the redox-probes can not reach the ITO electrode, Fig. 6.

Based on these results, it can be concluded that the protic ionic liquid HC_{16}imCl does not contribute with an own templating function under the reaction conditions of the EASA method investigated here. Indeed, the increased ratio of HC_{16}imCl in the HC_{16}imCl/C_{16}mimCl mixture resulted in a progressively less ordered pore structure. In a previous work published by us, it was suggested that when C_{16}mimCl forms channel-like pores in the silica network deposited *via* EASA the $C_{16}mim^+$ cation is electrostatically attracted to the network-forming and negatively charged silicate oligomers, which is vital for the entire templating process [28]. Based on this, the unsuitability of the HC_{16}imCl can be rationalized by the deprotonation of the imidazolium head, which may occur before or during EASA. The former case is compatible with the observed lower solubility of HC_{16}imCl as discussed above, while the latter is suggested based on the nature of the recorded chronoamperograms, Fig. 7. These chronoamperograms are in support for the latter case (i.e. deprotonation during EASA), since for the 30H/MC16 0.32 G sample they display an additional current during the first 5 s of deposition. This indicates the superposition of another reduction reaction (along with water electrolysis), which may plausibly originate from the reduction of the $HC_{16}im^+$ cations [48].

4. Conclusions

Through this work, we have been able to fill a previous knowledge gap regarding the suitability of long-chain ionic liquids, i.e. Im-SAILs, as templating agents during the formation of mesoporous structures. More specifically, we have considered the synthesis of porous thin films with vertically oriented and hexagonally ordered mesochannels. A variety of alkylimidazolium ionic liquids have been used with the aim to understand the effect of varying (i) the alkyl chain length, (ii) the metal substrate and (iii) the protic/aprotic character of the ionic liquid. The main results are summarized below.

Infrared, X-ray and voltammetric results clearly converge and allow stating that both C_{16}mimCl and C_{14}mimCl are efficient templating agents, while C_{12}mimCl fails in providing this function. This finding is in absolute line with what had been found for the CTAB family before. An interesting detail is that the cell parameter, and hence the pore size, decreases consistently with the shorter chain length, i.e. when changing C_{16}mimCl for C_{14}mimCl. This result implies that the pore size in mesoporous materials can be fine tuned by choosing the appropriate alkyl-methylimidazolium ionic liquid. With respect to the type of substrate used during deposition, we find that when using the ionic liquid C_{16}mimCl morphologically equivalent thin films can be deposited on both gold and ITO. However, the cell parameter of the hexagonally ordered pores increases with the cathodic current recorded during EASA. Finally, the possible role of a long-chain and protic ionic liquid as a templating agent has been investigated. By using mixtures of HC_{16}imCl and C_{16}mimCl we find that an increasing amount of the protic ionc liquid HC_{16}imCl has a negative effect on the pore ordering. This inefficiency may be correlated to the electrochemical instability of this protic ionic liquid under the cathodic potential used for deposition (-1.6 V on gold), which may cause the reduction of the imidazolium cations.

Declaration of Competing Interest

The authors declare that they have no known competing financial interests or personal relationships that could have appeared to influence the work reported in this paper.

Acknowledgements

The authors acknowledge the financial support from the Swedish Foundation for Strategic Research (SSF, FFL-16 0092 grant). The Chalmers Materials Analysis Laboratory (CMAL) is also acknowledged for providing instrumental time to perform X-ray scattering measurements.

Appendix A. Supplementary material

Supplementary data associated with this article can be found, in the online version, at https://doi.org/10.1016/j.molliq.2022.118686.

References

[1] H. Cao, Y. Hu, W. Xu, Y. Wang, X. Guo, Recent progress in the assembly behavior of imidazolium-based ionic liquid surfactants, J. Mol. Liq. 319 (2020) 114354, https://doi.org/10.1016/j.molliq.2020.114354, URL: https://doi.org/10.1016/j.molliq.2020.114354, ISSN 01677322.
[2] M.H. Anthofer, M.E. Wilhelm, M. Cokoja, I.I. Markovits, A. Pöthig, J. Mink, W.A. Herrmann, F.E. Kühn, Cycloaddition of CO2 and epoxides catalyzed by imidazolium bromides under mild conditions: Influence of the cation on catalyst activity, Catal. Sci. Technol. 4 (6) (2014) 1749–1758, https://doi.org/10.1039/c3cy01024d, ISSN 20444761.
[3] Y. Su, J. Yan, M. Li, M. Zhang, B. Mao, Electric double layer of Au(100)/imidazolium-based ionic liquids interface: Effect of cation size, J. Phys. Chem. C 117 (1) (2013) 205–212, https://doi.org/10.1021/jp3079919, ISSN 19327447.
[4] K. Goossens, K. Lava, C.W. Bielawski, K. Binnemans, Ionic Liquid Crystals: Versatile Materials, Chem. Rev. 116 (8) (2016) 4643–4807, https://doi.org/10.1021/cr400334b, ISSN 15206890.
[5] A. Vioux, B. Coasne, From Ionogels to Biredox Ionic Liquids: Some Emerging Opportunities for Electrochemical Energy Storage and Conversion Devices, Advanced Energy Materials 7 (22) (2017) 1–13, https://doi.org/10.1002/aenm.201700883, ISSN 16146840.
[6] R. Dutta, S. Kundu, N. Sarkar, Ionic liquid-induced aggregate formation and their applications, Biophysical Reviews 10 (3) (2018) 861–871, https://doi.org/10.1007/s12551-018-0408-5, ISSN 18672469.
[7] M. Blesic, M.H. Marques, N.V. Plechkova, K.R. Seddon, L.P.N. Rebelo, A. Lopes, Self-aggregation of ionic liquids: Micelle formation in aqueous solution, Green Chem. 9 (5) (2007) 481–490, https://doi.org/10.1039/b615406a, ISSN 14639262.
[8] C.M. Gordon, J.D. Holbrey, A.R. Kennedy, K.R. Seddon, Ionic liquid crystals: Hexafluorophosphate salts, J. Mater. Chem. 8 (12) (1998) 2627–2636, https://doi.org/10.1039/a806169f, ISSN 09599428.
[9] C.J. Bowlas, D.W. Bruceb, K.R. Seddon, Liquid-crystalline ionic liquids (1996) 1625–1626.
[10] T.L. Greaves, C.J. Drummond, Protic Ionic Liquids: Evolving Structure-Property Relationships and Expanding Applications, Chem. Rev. 115 (20) (2015) 11379–11448, https://doi.org/10.1021/acs.chemrev.5b00158, ISSN 15206890.
[11] S. Pan, M. Yao, J. Zhang, B. Li, C. Xing, X. Song, P. Su, H. Zhang, Recognition of Ionic Liquids as High-Voltage Electrolytes for Supercapacitors, Frontiers in

Chemistry 8 (May) (2020) 1–18, https://doi.org/10.3389/fchem.2020.00261, ISSN 22962646.
[12] T. Stettner, A. Balducci, Protic ionic liquids in energy storage devices: past, present and future perspective, Energy Storage Materials 40 (February) (2021) 402–414, https://doi.org/10.1016/j.ensm.2021.04.036, URL: https://doi.org/10.1016/j.ensm.2021.04.036. ISSN 24058297.
[13] L. Xiao, D. Su, C. Yue, W. Wu, Protic ionic liquids: A highly efficient catalyst for synthesis of cyclic carbonate from carbon dioxide and epoxides, Journal of CO2 Utilization 6 (2014) 1–6, https://doi.org/10.1016/j.jcou.2014.01.004, URL: https://doi.org/10.1016/j.jcou.2014.01.004. ISSN 22129820.
[14] J. Ingenmey, S. Gehrke, B. Kirchner, How to Harvest Grotthuss Diffusion in Protic Ionic Liquid Electrolyte Systems, ChemSusChem 11 (12) (2018) 1900–1910, https://doi.org/10.1002/cssc.201800436, ISSN 1864564X.
[15] J. Le Bideau, L. Viau, A. Vioux, Ionogels, ionic liquid based hybrid materials, Chem. Soc. Rev. 40 (2) (2011) 907–925, https://doi.org/10.1039/c0cs00059k, ISSN 14604744.
[16] Q. Su, Y. Qi, X. Yao, W. Cheng, L. Dong, S. Chen, S. Zhang, Ionic liquids tailored and confined by one-step assembly with mesoporous silica for boosting the catalytic conversion of CO2 into cyclic carbonates, Green Chem. 20 (14) (2018) 3232–3241, https://doi.org/10.1039/c8gc01038b, ISSN 14639270.
[17] L. Pang, R. Pang, L. Ge, L. Zheng, J. Zhao, H. Zhang, Trace determination of organophosphate esters in environmental water samples with an ionogel-based nanoconfined ionic liquid fiber coating for solid-phase microextraction with gas chromatography and flame photometric detection, J. Sep. Sci. 39 (22) (2016) 4415–4421, https://doi.org/10.1002/jssc.201600662, ISSN 16159314.
[18] K. Yavir, Ł. Marcinkowski, R. Marcinkowska, J. Namieśnik, A. Kloskowski, Analytical applications and physicochemical properties of ionic liquid-based hybrid materials: A review, Anal. Chim. Acta 1054 (2019) 1–16, https://doi.org/10.1016/j.aca.2018.10.061, ISSN 18734324.
[19] M.N. Garaga, V. Dracopoulos, U. Werner-Zwanziger, J.W. Zwanziger, M. Maréchal, M. Persson, L. Nordstierna, A. Martinelli, A long-chain protic ionic liquid inside silica nanopores: Enhanced proton mobility due to efficient self-assembly and decoupled proton transport, Nanoscale 10 (26) (2018) 12337–12348, https://doi.org/10.1039/c8nr02031k, ISSN 20403372.
[20] J. Alemán, A.V. Chadwick, J. He, M. Hess, K. Horie, R.G. Jones, P. Kratochvíl, I. Meisel, I. Mita, G. Moad, S. Penczek, R.F. Stepto, Definitions of terms relating to the structure and processing of sols, gels, networks, and inorganic-organic hybrid materials (IUPAC recommendations 2007), Pure Appl. Chem. 79 (10) (2007) 1801–1829, https://doi.org/10.1351/pac200779101801, ISSN 00334545.
[21] M. Thommes, K. Kaneko, A.V. Neimark, J.P. Olivier, F. Rodriguez-Reinoso, J. Rouquerol, K.S. Sing, Physisorption of gases, with special reference to the evaluation of surface area and pore size distribution (IUPAC Technical Report), Pure Appl. Chem. 87 (9–10) (2015) 1051–1069, https://doi.org/10.1515/pac-2014-1117, ISSN 13653075.
[22] M. Antonietti, D. Kuang, B. Smarsly, Y. Zhou, Ionic liquids for the convenient synthesis of functional nanoparticles and other inorganic nanostructures, Angewandte Chemie - International Edition 43 (38) (2004) 4988–4992, https://doi.org/10.1002/anie.200460091, ISSN 14337851.
[23] Y. Zhou, M. Antonietti, Preparation of highly ordered monolithic super-microporous lamellar silica with a room-temperature ionic liquid as template via the nanocasting technique, Adv. Mater. 15 (17) (2003) 1452–1455, https://doi.org/10.1002/adma.200305265, ISSN 09359648.
[24] Y. Zhou, J.H. Schattka, M. Antonietti, Room-temperature ionic liquids as template to monolithic mesoporous silica with wormlike pores via a sol-gel nanocasting technique, Nano Lett. 4 (3) (2004) 477–481, https://doi.org/10.1021/nl025861f, ISSN 15306984.
[25] J. Zhang, Y. Ma, F. Shi, L. Liu, Y. Deng, Room temperature ionic liquids as templates in the synthesis of mesoporous silica via a sol-gel method, Microporous Mesoporous Mater. 119 (1–3) (2009) 97–103, https://doi.org/10.1016/j.micromeso.2008.10.003, ISSN 13871811.
[26] T. Wang, H. Kaper, M. Antonietti, B. Smarsly, Templating behavior of a long-chain ionic liquid in the hydrothermal synthesis of mesoporous silica, Langmuir 23 (3) (2007) 1489–1495, https://doi.org/10.1021/la062470y, ISSN 07437463.
[27] Y. Zhou, M. Antonietti, A Series of Highly Ordered, Super-Microporous, Lamellar Silicas Prepared by Nanocasting with Ionic Liquids, Chem. Mater. 16 (3) (2004) 544–550, https://doi.org/10.1021/cm034442w, ISSN 08974756.
[28] S. Vavra, N. Vilà, A. Lotsari, A. Walcarius, A. Martinelli, An imidazolium ionic liquid as effective structure-directing agent for the fabrication of silica thin films with vertically aligned nanochannels, Microporous and Mesoporous Materials (June), doi:10.1016/j.micromeso.2020.110407. ISSN 13871811.
[29] H. Zhang, S. Liu, Preparation of ordered mesoporous silica materials templated by ionic liquids in alkaline condition, J. Porous Mater. 26 (1) (2019) 1–6, https://doi.org/10.1007/s10934-018-0600-9, URL: https://doi.org/10.1007/s10934-018-0600-9. ISSN 15734854.
[30] S. Vavra, K. Elamin, L. Evenäs, A. Martinelli, Transport Properties and Local Structure of an Imidazole/Protic Ionic Liquid Mixture Confined in the Mesopores of Hydrophobic Silica, J. Phys. Chem. C 125 (4) (2021) 2607–2618, https://doi.org/10.1021/acs.jpcc.0c08627, ISSN 19327455.
[31] G. Giordano, N. Vilà, E. Aubert, J. Ghanbaja, A. Walcarius, Multi-layered, vertically-aligned and functionalized mesoporous silica films generated by sequential electrochemically assisted self-assembly, Electrochim. Acta 237 (2017) 227–236, https://doi.org/10.1016/j.electacta.2017.03.220, URL: https://doi.org/10.1016/j.electacta.2017.03.220. ISSN 00134686.
[32] A. Walcarius, E. Sibottier, M. Etienne, J. Ghanbaja, Electrochemically assisted self-assembly of mesoporous silica thin films, Nat. Mater. 6 (8) (2007) 602–608, https://doi.org/10.1038/nmat1951.
[33] E. Sibottier, S. Sayen, F. Gaboriaud, A. Walcarius, Factors affecting the preparation and properties of electrodeposited silica thin films functionalized with amine or thiol groups, Langmuir 22 (20) (2006) 8366–8373, https://doi.org/10.1021/la060984r, ISSN 07437463.
[34] S. Hudson, D.A. Tanner, W. Redington, E. Magner, K. Hodnett, S. Nakahara, Quantitative TEM analysis of a hexagonal mesoporous silicate structure, PCCP 8 (29) (2006) 3467–3474, https://doi.org/10.1039/b605581h, ISSN 14639076.
[35] T. Rajkumar, G. Ranga Rao, Synthesis and characterization of hybrid molecular material prepared by ionic liquid and silicotungstic acid, Mater. Chem. Phys. 112 (3) (2008) 853–857, https://doi.org/10.1016/j.matchemphys.2008.06.046, ISSN 02540584.
[36] P. Innocenzi, Infrared spectroscopy of sol – gel derived silica-based films: a spectra-microstructure overview, J. Non-Cryst. Solids 316 (2003) 309–319.
[37] R. Lenza, W. Vasconcelos, Structural evolution of silica sols modified with formamide, Materials Research 4 (3) (2001) 175–179, https://doi.org/10.1590/s1516-14392001000300006, ISSN 1980-5373.
[38] E.M. Björk, P. Mäkie, L. Rogström, A. Atakan, N. Schell, M. Odén, Formation of block-copolymer-templated mesoporous silica, J. Colloid Interface Sci. 521 (2018) 183–189, https://doi.org/10.1016/j.jcis.2018.03.032, ISSN 10957103.
[39] S. Portal, R.M. Almeida, Variable incidence infrared absorption spectroscopy of gel-derived silica and titania films, Physica Status Solidi (A) Applied Research 201 (13) (2004) 2941–2947, https://doi.org/10.1002/pssa.200406846, ISSN 00318965.
[40] I.P. Lisovskii, V.G. Litovchenko, V.G. Lozinskii, G.I. Steblovskii, IR spectroscopic investigation of SiO2 film structure, Thin Solid Films 213 (2) (1992) 164–169, https://doi.org/10.1016/0040-6090(92)90278-J, ISSN 00406090.
[41] M. Zienkiewicz-Strzałka, M. Skibińska, S. Pikus, Small-angle X-ray scattering (SAXS) studies of the structure of mesoporous silicas, Nuclear Instruments and Methods in Physics Research, Section B: Beam Interactions with Materials and Atoms 411 (2017) 72–77, https://doi.org/10.1016/j.nimb.2017.03.028, ISSN 0168583X.
[42] J. Choi, I. Gunkel, Y. Li, Z. Sun, F. Liu, H. Kim, K.R. Carter, T.P. Russell, Macroscopically ordered hexagonal arrays by directed self-assembly of block copolymers with minimal topographic patterns, Nanoscale 9 (39) (2017) 14888–14896, https://doi.org/10.1039/c7nr05394k, URL: https://doi.org/10.1039/c7nr05394k. ISSN 20403372.
[43] Y. Guillemin, M. Etienne, E. Aubert, A. Walcarius, Electrogeneration of highly methylated mesoporous silica thin films with vertically-aligned mesochannels and electrochemical monitoring of mass transport issues, J. Mater. Chem. 20 (32) (2010) 6799–6807, https://doi.org/10.1039/c0jm00305k, ISSN 09599428.
[44] C. Karman, N. Vilà, A. Walcarius, Amplified Charge Transfer for Anionic Redox Probes through Oriented Mesoporous Silica Thin Films, ChemElectroChem 3 (12) (2016) 2130–2137, https://doi.org/10.1002/celc.201600303, ISSN 21960216.
[45] A. Goux, M. Etienne, E. Aubert, C. Lecomte, J. Ghanbaja, A. Walcarius, Oriented mesoporous silica films obtained by electro-assisted self-assembly (EASA), Chem. Mater. 21 (4) (2009) 731–741, https://doi.org/10.1021/cm8029664, ISSN 08974756.
[46] S.P. Moulik, M.E. Haque, P.K. Jana, A.R. Das, Micellar properties of cationic surfactants in pure and mixed states, J. Phys. Chem. 100 (2) (1996) 701–708, https://doi.org/10.1021/jp9506494, ISSN 00223654.
[47] I. Garcia-Mateos, M.M. Velazquez, L.J. Rodriguez, Critical Micelle Concentration Determination in Binary Mixtures of Ionic Surfactants by Deconvolution of Conductivity/Concentration Curves, Langmuir 6 (6) (1990) 1078–1083, https://doi.org/10.1021/la00096a009, ISSN 15205827.
[48] T. Stettner, F.C. Walter, A. Balducci, Imidazolium-Based Protic Ionic Liquids as Electrolytes for Lithium-Ion Batteries, Batteries & Supercaps 2 (1) (2019) 55–59, https://doi.org/10.1002/batt.201800096.